

# Lithium storage study on MoO<sub>3</sub>-grafted TiO<sub>2</sub> nanotube arrays

Tauseef Anwar<sup>1</sup> · Li Wang<sup>1</sup> · Li Jiaoyang<sup>1</sup> · Wang Chen<sup>2</sup> · Rizwan Ur Rehman Sagar<sup>3</sup> · Liang Tongxiang<sup>2</sup>

Received: 8 January 2016 / Accepted: 27 February 2016 / Published online: 16 March 2016  
© The Author(s) 2016. This article is published with open access at Springerlink.com

**Abstract** Titanium dioxide nanotube arrays (TNAs) were fabricated via anodic ionization. Porous MoO<sub>3</sub> was grafted on TNAs with the help of hydrothermal method. Scanning electron microscopy and X-ray powder diffraction was utilized for the confirmation of one dimensional morphology and phase identification. The porous MoO<sub>3</sub> nanoflake-grafted TNAs (MoO<sub>3</sub>/TNAs) electrode was used as anode material in lithium ion battery (LIB) and it was found that the areal specific capacity of MoO<sub>3</sub>/TNAs ( $\sim 797 \mu\text{Ah cm}^{-2}$ ) was three times higher than those of anatase TNAs ( $\sim 287 \mu\text{Ah cm}^{-2}$ ) and porous MoO<sub>3</sub> ( $\sim 234 \mu\text{Ah cm}^{-2}$ ) at  $50 \mu\text{A cm}^{-2}$ .

**Keywords** Molybdenum oxide · Titanium dioxide nanotube arrays (TNAs) · Anode · Lithium-ion batteries (LIBs)

## Introduction

Lithium ion battery (LIB) is one of the most reliable power sources for portable electronic devices. The improved performance of microbatteries is highly necessary for modern microelectronic devices such as PC memory, microelectromechanical systems (MEMS), medical implants, hearing aids, “smart” cards, RF-ID tags, remote sensors and energy harvesters, etc. (Kyeremateng 2014; Matiko et al. 2014; Patil et al. 2008; Pikul et al. 2013). The requirement of high-performance LIBs encourages scientists to develop new anode materials with capacity higher than graphite (Reddy et al. 2013; Wu et al. 2012a; Wu and Hong 2014; Xiong et al. 2014). TiO<sub>2</sub> is a promising material for lithium storage due to its low volume expansion, environmental benignity and widespread availability. Amongst the various nanostructures of TiO<sub>2</sub> (Armstrong et al. 2006; Cao et al. 2010; Liu et al. 2012; Qiu et al. 2010; Ren et al. 2012; Wang et al. 2011), titanium dioxide nanotube arrays (TNAs) (Guo et al. 2012) are favorable due to their high specific surface area, high porosity, vertical orientation which accommodate volume expansion and also provide short lithium ion diffusion path (Wu et al. 2012b). However, the areal specific capacity, even for the optimized TNAs, is found to be low (Tauseef Anwar et al. 2015). Three different methods have been proposed to enhance the specific capacity: (1) doping TNAs with metal or nonmetal elements (Kyeremateng et al. 2013b; Liu et al. 2008, 2009); (2) coating TNAs with conductive reagents (Guan and Wang 2013; Kim et al. 2010; Zhang et al. 2009); (3) modify TNAs with oxide materials that have larger capacities [SnO<sub>2</sub> (Meng et al. 2013), Co<sub>3</sub>O<sub>4</sub> (Fan et al. 2013; Kyeremateng et al. 2013a), Nb<sub>2</sub>O<sub>5</sub> (Yang et al. 2013) and Fe<sub>2</sub>O<sub>3</sub> (Yu et al. 2013)] to yield hybrid or composite structures.

**Electronic supplementary material** The online version of this article (doi:10.1007/s13204-016-0526-y) contains supplementary material, which is available to authorized users.

✉ Liang Tongxiang  
txliang@tsinghua.edu.cn

<sup>1</sup> Beijing Key Lab of Fine Ceramics, Institute of Nuclear and New Energy Technology, Tsinghua University, Beijing 100084, People’s Republic of China

<sup>2</sup> State Key Lab of New Ceramic and Fine Processing, Tsinghua University, Beijing 100084, People’s Republic of China

<sup>3</sup> Nanshan District Key Lab for Biopolymers and Safety Evaluation, College of Materials Science and Engineering, Shenzhen University, Shenzhen 518060, People’s Republic of China

MoO<sub>3</sub> is an anode material candidate due to its high theoretical capacity (1117 mAh g<sup>-1</sup>). The orthorhombic phase layered structure of α-MoO<sub>3</sub> hosts Li<sup>+</sup> by insertion and deinsertion reaction. However, the electrochemical properties of TNAs could be further enhanced with the extra porous hybrid material such as MoO<sub>3</sub> (Fan et al. 2013; Guan et al. 2014a, b; Kyeremateng et al. 2013a; Meng et al. 2013; Wang et al. 2013; Xue et al. 2011; Zhu et al. 2015). Considering low electronic conductivity and high volume expansion, Yu et al. (2014) synthesized porous MoO<sub>3</sub> thin films and elucidated better performance as compared to bulk MoO<sub>3</sub>. Zhao et al. (2013) synthesized porous MoO<sub>3</sub> thin films via electro-deposition which exhibit a high capacity of 650 mAh g<sup>-1</sup> at high current density of 3 A g<sup>-1</sup>. Yu et al. synthesized porous MoO<sub>3</sub> nanosheets by hydrothermal method at Ti substrate and the nanosheets showed specific capacity of 750 mAh g<sup>-1</sup> at 1C-rate. There are rare reports on the MoO<sub>3</sub>/TNAs as anode material in LIBs. However, different fabrication of coating MoO<sub>3</sub> on TNAs led difference in their electrochemical properties. The hydrothermal synthesis for the grafting of MoO<sub>3</sub> nanoflakes at TNAs was used first time. The fabrication method and porosity would play important role for future electrochemical properties of material.

Herein, TNAs were grown at Ti substrate and consecutive annealing transforms TNAs in anatase phase. The porous MoO<sub>3</sub> were grafted using a facile hydrothermal method which facilitate high yield product (Fig. 1) (Fan et al. 2015a, b; Gong et al. 2015). The grafting of porous

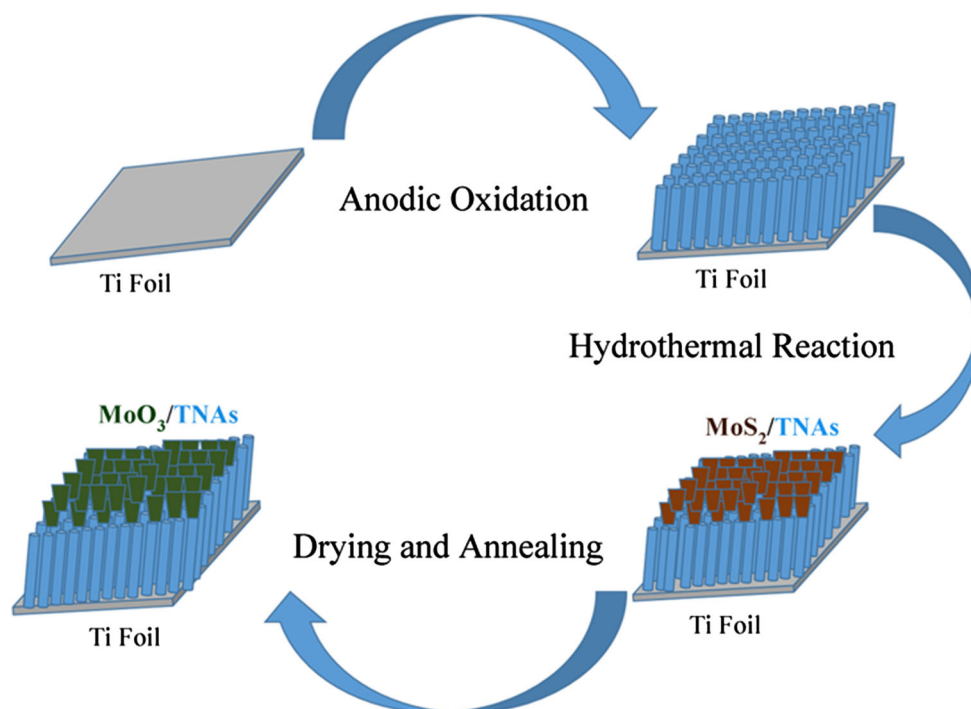
MoO<sub>3</sub> nanoflakes at TNAs was controlled via hydrothermal reaction time. The electrochemical properties were optimized by controlling thickness of MoO<sub>3</sub> with hydrothermal duration. There are several benefits of utilizing MoO<sub>3</sub>/TNAs as electrode in LIBs. Firstly, TiO<sub>2</sub> with zero strain (ca. 4 % volume change after lithiation) is an ideal material to optimize cycle stability and rate performance. Secondly, the nanosize and intrinsic characteristics of porous MoO<sub>3</sub> will provide both reversible large capacity and good electrical conductivity. Thirdly, the specific architectural feature of binder-free single-crystalline TiO<sub>2</sub> nanotube array will simplify the electrode fabrication process. Fourthly, TiO<sub>2</sub> nanotube array provides direct electron transport pathway between active material and current collector and also facilitate uniform deposition of porous MoO<sub>3</sub> with large areal mass loading. In contrast to the advantages, there are disadvantages as well, firstly, to get synergic capacity of both anatase TNAs and porous MoO<sub>3</sub> the potential window must be higher (0.005–3 V). Secondly, the solid electrolyte interface (SEI) layer is inevitable which leads to high capacity fading.

## Experimental section

### Synthesis of MoO<sub>3</sub>/TNAs

Prior to anodic oxidation, titanium foil (0.125-mm-thick foil, 99.7 % purity, Sigma Aldrich) was degreased by

**Fig. 1** Schematic illustration of the formation of MoO<sub>3</sub>/TNAs composite: (I) Ti substrate; (II) formation of TNAs on Ti substrate; (III) grafting MoS<sub>2</sub> on TNAs via hydrothermal reaction (IV) formation of MoO<sub>3</sub>/TNAs



sonication in acetone, ethanol and deionized water in turn, then dried in air. The electrochemical cell for anodization was a two-electrode cell, consisting of Ti foil as working electrode and platinum foil as counter electrode. Electrochemical anodization experiments were conducted at a constant potential with a DC power supply (DH1722A-2 110V/3A). The electrolyte was 0.3 wt%  $\text{NH}_4\text{F}$  and 2 vol.% water in ethylene glycol (99.8 %, anhydrous). All the tests were performed at room temperature. The TNAs were synthesized at the voltage of 50 V for 2 h. The as-prepared TNAs were annealed at 450 °C to transform its phase.

The porous  $\text{MoO}_3$  were deposited by hydrothermal method reported elsewhere (Yu et al. 2014). The TNAs containing Ti substrate was placed against the wall of Teflon liner with interested surface downwards. The prepared 30 mL solution of  $(\text{NH}_4)_6\text{Mo}_7\text{O}_{24}\cdot 4\text{H}_2\text{O}$  (1 mmol) and thiourea (0.484 g) was transferred gently in Teflon-lined stainless steel autoclaves. Hereafter, the autoclave was sealed and maintained at 180 °C for different reaction time (2, 4, 6, 8, 10 h) and cooled down to room temperature spontaneously. The samples were collected and rinsed with distilled water for several times to remove the residual reactant and dried in vacuum oven at 80 °C for 30 min. Now  $\text{MoS}_2$ -deposited TNAs were obtained and annealed at 400 °C for 2 h to convert  $\text{MoS}_2$  into  $\text{MoO}_3$ . For comparison, porous  $\text{MoO}_3$  were grown in the similar way at titanium substrate.

## Characterization

The surface and cross-sectional morphologies of the TNAs and  $\text{MoO}_3/\text{TNAs}$  were characterized using field emission scanning electron microscopy (FE-SEM LEO 1530). The phase structure of the TNAs, porous  $\text{MoO}_3$  and  $\text{MoO}_3/\text{TNAs}$  were characterized by X-ray powder diffraction (XRD). The  $\text{Cu K}\alpha$  radiation ( $\lambda = 0.15$  nm) were used for XRD analysis. The electrochemical kinetics were studied by cyclic voltammetry (CV) test measured at a scan rate of  $5$  mV  $\text{s}^{-1}$  at a potential between 0 and 3 V.

## Electrochemical characterization

The lithium storage performances of electrode were evaluated using  $\text{Li}|\text{MoO}_3/\text{TNAs}$  half-cells. The cells were 2032 coin cell and assembled in an argon-filled glove box. The cathode was  $\text{MoO}_3/\text{TNAs}$  without additives, the anode was lithium foil, and the separator is celgard 2300. The electrolyte is 1 M  $\text{LiPF}_6$  dissolved in the mixture of ethylene carbonate (EC) and dimethyl carbonate (DMC) with volume ratio of 1:1. The cells were galvanostatically charged and discharged between 0.005 and 3 V (vs.  $\text{Li}/\text{Li}^+$ ) at the current of 0.01 mA for the initial two cycles and then at 0.05 mA for the following cycles. The electrodes for

comparison were configured and analyzed at same parameters.

## Results and discussion

The synthesis process of porous  $\text{MoO}_3/\text{TNAs}$  is schematically illustrated in Fig. 1. Well oriented TNAs are synthesized at the nanostructured substrate via electrochemical anodization of Ti foil at room temperature (Fig. 1 I and II).  $\text{MoS}_2$  is coated on the top of these vertical TNAs via hydrothermal reaction (Fig. 1 III) and oxygen annealing converts  $\text{MoS}_2$  in  $\text{MoO}_3$  (Fig. 1 IV).

The annealed TNAs and  $\text{MoO}_3/\text{TNAs}$  are characterized by SEM, as shown in supporting information Fig. S1 and S2, respectively. It is found that the TNAs were compact and uniform, without secondary nanostructures on the top or side surface (Fig. S1). The average inner diameter of the TNAs is around 60 nm and the length was about 3–5  $\mu\text{m}$ . For  $\text{MoO}_3/\text{TNAs}$  sample,  $\text{MoO}_3$  nanoflakes are grafted on the top of TNAs and the thickness of  $\text{MoO}_3$  is controlled via deposition time (Fig. S2). The  $\text{MoO}_3$  precipitate coat the surface partially when hydrothermal reaction was continued for 2 h (Fig. S2a) and the side of TNAs was almost as neat as pristine TNAs (inset Fig. S2b). As the hydrothermal duration increases to 4 h, both the top surface and side surface of TNAs are fully covered with  $\text{MoO}_3$  nanoflakes and nanochannels were blocked (Fig. S2c, d). The  $\text{MoO}_3$  nanoflakes with various lateral dimensions ranging in nanometers are grafted on the top, inner and outer surface of TNAs. The coating layer thickness increased linearly as reaction time increased as shown in Fig. S2. The TNAs might incorporate  $\text{MoO}_3$  for stacking and control volumetric changes on lithiation.  $\text{MoO}_3$  nanoflakes due to their 2D structure and high surface area can facilitate the transport of ions/electrons thus improve the response of system and recovery kinetics (Alsaif et al. 2014) (Fig. 2).

The  $\alpha$ - $\text{MoO}_3$  is an anode material candidate for LIBs due to its stable layer structure which facilitates lithium insertion. The XRD pattern of  $\text{MoO}_3/\text{TNAs}$  indicates that diffraction peaks could be indexed to titanium (JCPDS NO. 44-1294), tetragonal anatase  $\text{TiO}_2$  (JCPDS no. 21-1272) and orthorhombic  $\alpha$ - $\text{MoO}_3$  (JCPDS no. 05-0508) (Fig. 2; Fig. S4). In detail, the peaks at 35°, 38.4°, 40.1°, 53°, 62.9°, 70.6°, 74.1°, 76.2° and 77.4° represent Ti planes (100), (002), (101), (102), (110), (103), (200), (112) and (201), respectively. The peaks at 12.6°, 23.3°, 27.3° and 33.7°, can be attributed to  $\alpha$ - $\text{MoO}_3$  (020), (110), (021), and (111) planes, respectively. The peaks at 25.0° and 47.9° can be attributed to (101) and (200) planes of anatase- $\text{TiO}_2$ . The  $\text{MoO}_3$  peak (040) at 25.7 overlaps with  $\text{TiO}_2$  in composite. The anatase  $\text{TiO}_2$  peaks could be observed in

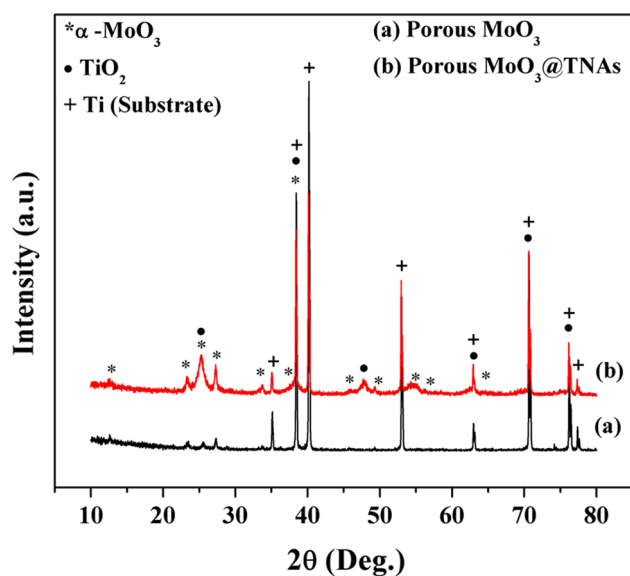


**Fig. 2** XRD patterns of (a) porous MoO<sub>3</sub> (b) MoO<sub>3</sub>/TNAs composite

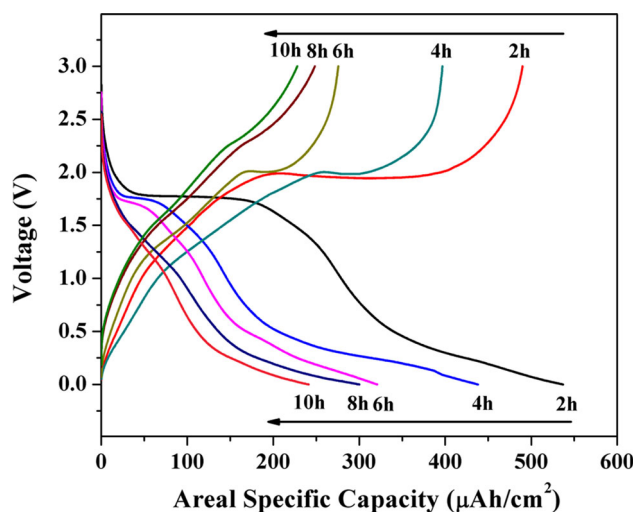


**Fig. 3** The 3rd charge and discharge curves of MoO<sub>3</sub>/TNAs synthesized for 2, 4, 6, 8 and 10 h at current density of 50 μA cm<sup>-2</sup> at a potential of 0.005–3 V

only MoO<sub>3</sub>/TNAs composite and porous MoO<sub>3</sub> did not show any anatase TiO<sub>2</sub> peak. The XRD of MoO<sub>3</sub>/TNAs with standard data is shown in Fig. S4. These results suggest that adopted synthesis strategy successfully covers anatase TNAs with α-MoO<sub>3</sub> having good crystallinity without introducing other impurity phases.

The TNAs with fully covered surface may hinder Li<sup>+</sup> ion and electron recombination due to slow movement of electrons from oxide material which have low conductivity. As the thickness of coated oxide material increases, the movement of electron is hindered and reduces lithium intercalation. The electrochemical properties of MoO<sub>3</sub>/TNAs synthesized for different times of 2–10 h were

elucidated in Fig. 3. As the deposited layer of nanoflakes thickens with increasing reaction time so capacity decreases, consistent with literature (Guan et al. 2014a; Zhu et al. 2015). The Li insertion and extraction plateau can be observed till 6 h time duration which indicates incorporation of TNAs, but length of plateau decreases with increase in time. The plateau for 8 and 10 h fully disappeared indicating that incorporation of anatase TNAs diminished after long time duration which is attributed to thickness of MoO<sub>3</sub> which might hinder electronic and ionic recombination.

To optimize the highest capacity, the hydrothermal reaction is conducted for 3 h (Fig. 4a, b). The top surface of TNAs was partially covered with MoO<sub>3</sub> and upper orifices remain uncovered not to block nanochannels which facilitate Li ions transportation to the inner wall of nanotubes (Fig. 4a). The lateral sides of TNAs were grafted with MoO<sub>3</sub> (Fig. 4b). A suitable amount of MoO<sub>3</sub> deposition on top of TNAs is required for the best performance as anode material.

Anatase TiO<sub>2</sub> has a tetragonal structure (space group I41/amd), in which a Ti<sup>4+</sup> ion is surrounded by a distorted oxygen octahedron while numerous vacant octahedral and tetrahedral sites exist between these octahedrons. Li ions are accommodated in these vacant sites. Two voltage plateaus appear near 1.7 and 1.9 V (vs. Li/Li<sup>+</sup>) in the curves of the anatase TNAs and MoO<sub>3</sub>/TNAs anodes, which demonstrate that TNAs are also contributing in MoO<sub>3</sub>/TNAs while they are totally different from porous MoO<sub>3</sub>. The one at 1.7 V (vs. Li/Li<sup>+</sup>) in the negative scan corresponds to Li-ion insertion into TiO<sub>2</sub>, while the other in the positive scan accords with Li-ion desorption. The total reaction for Li-ion insertion/extraction is described by (Guan et al. 2014a, b):



Here,  $x$  could be up to 0.5, corresponding to a capacity of 168 mAh g<sup>-1</sup>.

α-MoO<sub>3</sub> has an orthorhombic structure containing distorted MoO<sub>6</sub> octahedral. They share edges and form chains that are cross-linked through oxygen atoms to yield layers. The Li ions were accommodated in the interlayer space between these layers. Most of Li ions move easily, which is the cause of excellent reversibility. The total reaction for Li-ion insertion and extraction is described by (Guan et al. 2014a, b):



It is known that the electrochemical properties not only depends on surface properties and crystallinity, but also depends upon the texture (Fan et al. 2013). The nano-hybrid materials reduce Li ion diffusion path enabling electrolyte ions to be transported smoothly and pores

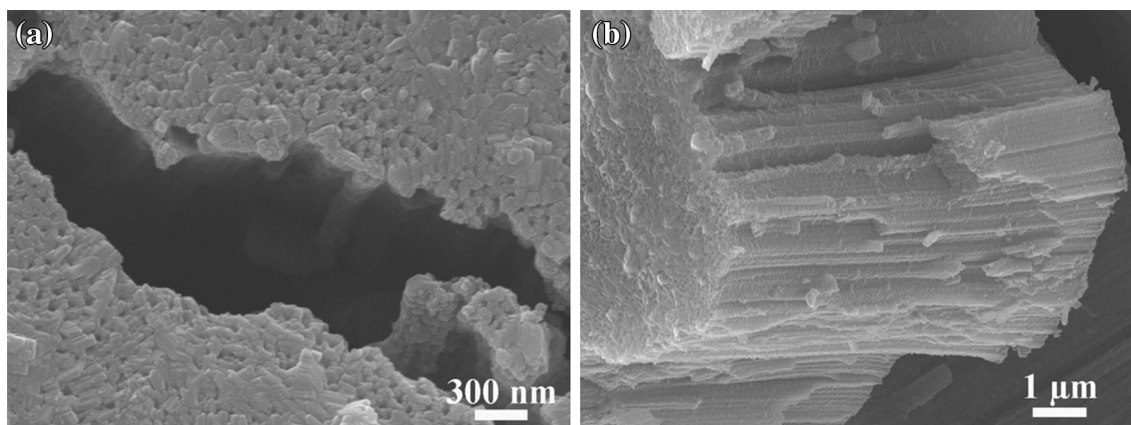
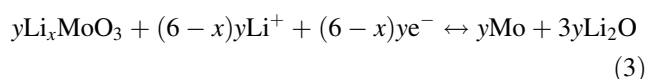


**Fig. 4** MoO<sub>3</sub>/TNAs for the time duration of 3 h: **a** top surface of TNAs, **b** lateral side of TNAs

provide large specific surface area which strongly suggests its potential applicability as an electrode material for LIBs (Moriguchi et al. 2006). The Li-ion intercalation behaviors of anatase TNAs, porous MoO<sub>3</sub> and MoO<sub>3</sub>/TiO<sub>2</sub> are compared to study the effect of MoO<sub>3</sub> according to their electrochemical properties (Fig. 5).

The reaction kinetics is studied with the help of CV measured at a scan rate of 5 mV s<sup>-1</sup> at 0–3 V, as shown in Fig. 5a–c. The cathodic peaks are observed at 0.6 and 1.45 V for the anatase TNAs, while 1.94 V for porous MoO<sub>3</sub> (Li et al. 2006; Ryu et al. 2012). The cathodic peaks for MoO<sub>3</sub>/TNAs are observed at 0.66 V corresponding to the reduction of electrolyte solution and formation of solid electrolyte interface (SEI) layer on the surface of working electrode. The anodic peaks observed for anatase TNAs at 2.37 V, for porous MoO<sub>3</sub> at 1.52 V while for MoO<sub>3</sub>/TNAs at 2.34 and 1.51 V were due to the delithiation from oxides (Li et al. 2006; Ryu et al. 2012).

The charge/discharge curves for the third cycle at current density of 50 μA cm<sup>-2</sup> at potential window of 0.005–3 V are shown in Fig. 5d. The first two charge/discharge cycles are measured at the current density of 10 μA cm<sup>-2</sup> to stabilize the charge and discharge. The third cycle discharge capacity is 287, 234 and 797 μAh cm<sup>-2</sup> for anatase TNAs, porous MoO<sub>3</sub> and MoO<sub>3</sub>/TNAs, respectively. The areal specific capacity for MoO<sub>3</sub>/TNAs is three times higher than those of anatase TNAs and porous MoO<sub>3</sub>. The electrochemical properties improve due to the combination of MoO<sub>3</sub> with high specific capacity and ordered TNAs with large surface area for efficient deposition and fast Li-ion kinetics. The anatase TiO<sub>2</sub> incorporating MoO<sub>3</sub> also helps to enhance capacity. A larger irreversible capacity is observed due to formation of SEI layer. The areal capacity increases when potential drops below 1.0 V. The slope below 0.7 V suggests Li ions intercalate into porous MoO<sub>3</sub> and MoO<sub>3</sub>/TiO<sub>2</sub> according to following reaction (Guan et al. 2014a, b):



Li ions insert into anatase TNAs or react with electrolyte as potential drops below 0.5 V. The lithiation in MoO<sub>3</sub>/TNAs appears in a different way. At lower voltage regions Li ions react with the solid solution (Li<sub>x</sub>MoO<sub>3</sub>) to form Mo metal and Li<sub>2</sub>O oxides which are irreversible, but the nano-textured synthesis induces a reversible reaction of Li<sub>2</sub>O during charging (Guan et al. 2014a, b).

Stable cyclic performance of electrode materials is important for practical application of lithium-ion batteries. Figure 6a depicts the cyclic performance and efficiency of anatase TNAs, porous MoO<sub>3</sub> and MoO<sub>3</sub>/TNAs. The initial two cycles are charged/discharged at the current density of 10 μA cm<sup>-2</sup> to stabilize the surface reactions and next charged/discharged cycles are at 50 μA cm<sup>-2</sup>. The cyclic performance of anatase TNAs and porous MoO<sub>3</sub> are approximately similar and stable after few cycles. The composite electrode shows considerably enhanced charge/discharge capacity with respect to anatase TNAs and porous MoO<sub>3</sub> electrodes during all the 50 cycles. The MoO<sub>3</sub>/TNAs nanostructure electrode exhibits a discharge capacity of 797 μAh cm<sup>-2</sup> for third cycle and is stable after 25th cycle till 50th cycle (226 μAh cm<sup>-2</sup>), which is much higher than those of the anatase TNAs, porous MoO<sub>3</sub> electrodes (84 and 129 μAh cm<sup>-2</sup> for 50th cycles, respectively). The high capacity fading in initial cycles of MoO<sub>3</sub>/TNAs might be attributed to the formation of SEI layer and conversion of Li<sub>2</sub>O oxides. The efficiency of all samples is 100 % (Fig. 6a).

The rate performance of the three samples is measured with different current densities (50, 100, 150, 200, 250 and again 50 μA cm<sup>-2</sup>). The rate capability of MoO<sub>3</sub>/TNAs is the highest compared to anatase TNAs and porous MoO<sub>3</sub>. After the current density switched back to 50 μA cm<sup>-2</sup>, the capacity for MoO<sub>3</sub>/TNAs is higher enough and more

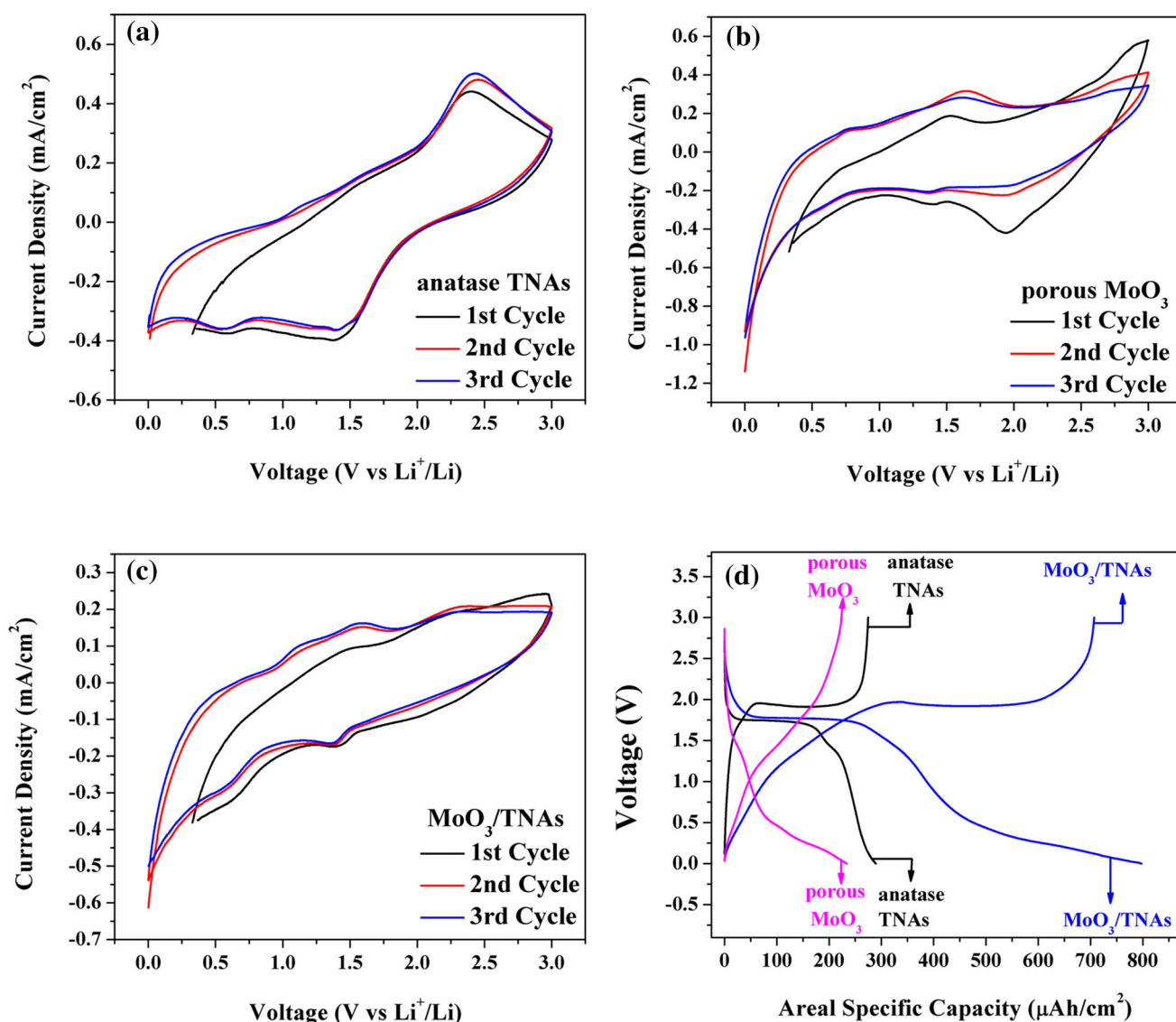


**Fig. 5** Cyclic voltammetry curves of the anataze TNAs (a), porous MoO<sub>3</sub> (b) and MoO<sub>3</sub>/TNAs (c), (d) the 3rd charge and discharge curve of anataze TNAs, porous MoO<sub>3</sub> and MoO<sub>3</sub>/TNAs at current density of 50 μA cm<sup>-2</sup> at a potential of 0.005–3 V

stable. These results reveal that the incorporation of anataze TiO<sub>2</sub> into MoO<sub>3</sub> nanostructures can greatly enhance the electrochemical performance for lithium storage.

The MoO<sub>3</sub>/TNAs may be used as anode material in LIBs for achieving high capacity. However, thickness of grafted MoO<sub>3</sub> could be changed for achieving optimal results. Previously reported results and our present results are summarized in Table 1. Firstly, there are rare reports about MoO<sub>3</sub>-grafted TNAs as anode material. The length of TNAs may play their role and specific capacity enhanced from 154.9 to 1340 μAh cm<sup>-2</sup> for 1.6 and 9 μm, MoO<sub>3</sub>-grafted TNAs, respectively. Although, specific capacity has been increased a lot, our results showed that MoO<sub>3</sub>-grafted

TNAs of small length (3 μm) exhibited higher specific capacity (797 μAh cm<sup>-2</sup>) as compared to reported literature. It might be due to the fabrication process, synergetic effect of MoO<sub>3</sub>-grafted TNAs and porous nature of MoO<sub>3</sub>. The hydrothermal method is a wet method which may be helpful for covering all the voids of TNAs. Therefore, MoO<sub>3</sub> may fill TNAs which results in the present electrochemical properties. The lithium ion inserted in MoO<sub>3</sub> first and combination of MoO<sub>3</sub> with TNAs enhanced the lithium insertion/deinsertion, which results in higher capacity than anataze TNAs. The thickness of MoO<sub>3</sub> can be varied via fabrication method which brings exciting controllable performance of LIBs.

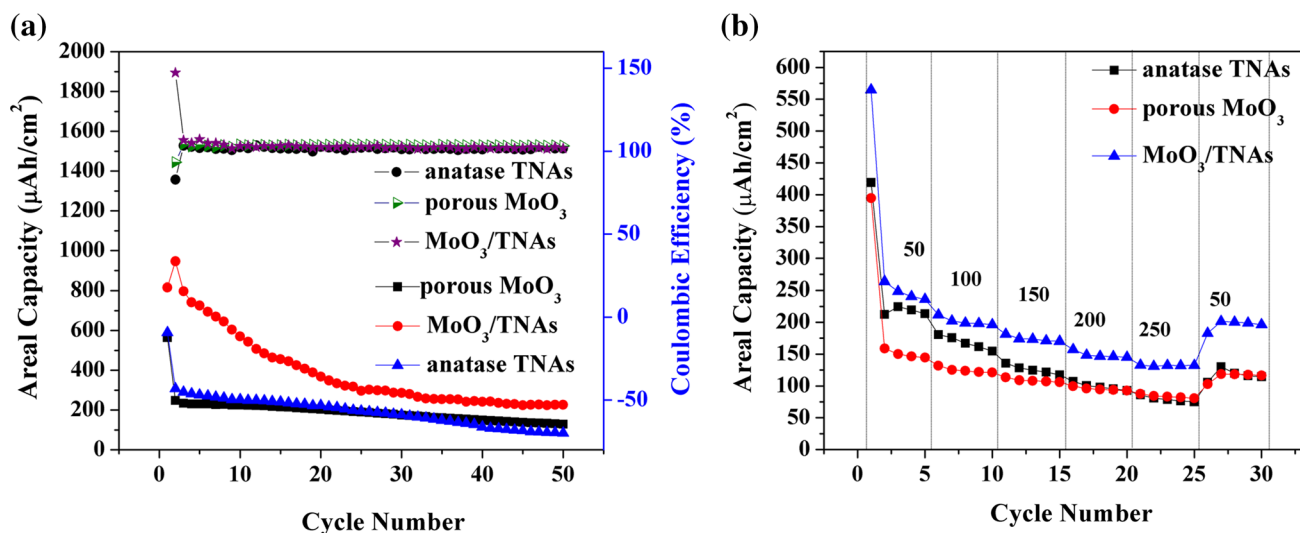


**Fig. 6** **a** The cyclic performance and efficiency of anatase TNAs, porous MoO<sub>3</sub> and MoO<sub>3</sub>/TNAs. **b** The rate performance of anatase TNAs, porous MoO<sub>3</sub>, MoO<sub>3</sub>/TNAs

**Table 1** Comparison of Guan et al. MoO<sub>3</sub>/TNAs and our synthesized MoO<sub>3</sub>/TNAs

Material	MoO <sub>3</sub> /TNAs (references)	MoO <sub>3</sub> /TNAs (our work)
Coating method	Electrochemical	Hydrothermal
Titanium dioxide nanotube arrays length (μm)	1.6–9	3–5
1st discharge capacity (μAh cm <sup>-2</sup> )	1340 at 800 μA cm <sup>-2</sup> (Guan et al. 2014a)	947 at 10 μA cm <sup>-2</sup>
3rd discharge capacity (μAh cm <sup>-2</sup> )	154.9 at 50 μA cm <sup>-2</sup> (Guan et al. 2014b)	797 at 50 μA cm <sup>-2</sup>

**Conclusion**

TNAs were grown via anodic oxidation method and MoO<sub>3</sub> nanoflakes were grafted at TNAs via hydrothermal method for the first time. The optimal electrochemical properties of MoO<sub>3</sub>/TNAs were obtained for 3 h deposition of MoO<sub>3</sub> nanoflakes. The specific capacity (~797 μAh cm<sup>-2</sup>) of MoO<sub>3</sub>/TNAs was three times higher than anatase TNAs (~287 μAh cm<sup>-2</sup>) and porous MoO<sub>3</sub> (~234 μAh cm<sup>-2</sup>). The rate performance and efficiency of LIB (in which MoO<sub>3</sub>/TNAs used as anode material) were also enhanced. The anatase TiO<sub>2</sub> incorporates MoO<sub>3</sub> nanostructures and enhances the electrochemical performance, hence MoO<sub>3</sub>/TNAs electrode might be a useful anode material for lithium ion micro-batteries. The carbon-free conducting nanocoated electrodes will be able to open new opportunities in the development of high-performance next-generation lithium-ion micro-batteries.

**Acknowledgments** This work is supported by the National Natural Science Foundation of China (Grant no. 21271114); Tsinghua University independent research and development fund (20111080982)

and Program for Changjiang Scholars and Innovative Research Team in University (IRT13026).

**Open Access** This article is distributed under the terms of the Creative Commons Attribution 4.0 International License (<http://creativecommons.org/licenses/by/4.0/>), which permits unrestricted use, distribution, and reproduction in any medium, provided you give appropriate credit to the original author(s) and the source, provide a link to the Creative Commons license, and indicate if changes were made.

**References**

Alsaif MMYA, Balendhran S, Field MR, Latham K, Wlodarski W, Ou JZ, Kalantar-zadeh K (2014) Two dimensional α-MoO<sub>3</sub> nanoflakes obtained using solvent-assisted grinding and sonication method: application for H<sub>2</sub> gas sensing. *Sens Actuators B* 192:196–204. doi:10.1016/j.snb.2013.10.107

Anwar T, Wang L, Tongxiang L, He X, Sagar RUR, Shehzad K (2015) Effect of aspect ratio of titanium dioxide nanotube arrays on the performance of lithium ion battery. *Int J Electrochem Sci* 10:6537–6547

Armstrong G, Armstrong AR, Bruce PG, Reale P, Scrosati B (2006) TiO<sub>2</sub>(B) nanowires as an improved anode material for lithium-ion batteries containing LiFePO<sub>4</sub> or LiNi<sub>0.5</sub>Mn<sub>1.5</sub>O<sub>4</sub> cathodes

- and a polymer electrolyte. *Adv Mater* 18:2597–2600. doi:10.1002/adma.200601232
- Cao F-F, Wu X-L, Xin S, Guo Y-G, Wan L-J (2010) Facile synthesis of mesoporous TiO<sub>2</sub> – C nanosphere as an improved anode material for superior high rate 1.5 V rechargeable Li ion batteries containing LiFePO<sub>4</sub> – C cathode. *J Phys Chem* 114:10308–10313. doi:10.1021/jp103218u
- Fan Y, Zhang N, Zhang L, Shao H, Wang J, Zhang J, Cao C (2013) Co3O4-coated TiO<sub>2</sub> nanotube composites synthesized through photo-deposition strategy with enhanced performance for lithium-ion batteries. *Electrochim Acta* 94:285–293. doi:10.1016/j.electacta.2013.01.114
- Fan J, Li G, Luo D, Fu C, Li Q, Zheng J, Li L (2015a) Hydrothermal-assisted synthesis of Li-rich layered oxide microspheres with high capacity and superior rate-capability as a cathode for lithium-ion batteries. *Electrochim Acta* 173:7–16. doi:10.1016/j.electacta.2015.05.028
- Fan JM, Li GS, Luo D, Fu CC, Li Q, Zheng J, Li LP (2015b) Hydrothermal-assisted synthesis of Li-rich layered oxide microspheres with high capacity and superior rate-capability as a cathode for lithium-ion batteries. *Electrochim Acta* 173:7–16. doi:10.1016/j.electacta.2015.05.028
- Gong J, Zeng W, Zhang H (2015) Hydrothermal synthesis of controlled morphologies of MoO<sub>3</sub> nanobelts and hierarchical structures. *Mater Lett* 154:170–172. doi:10.1016/j.matlet.2015.04.092
- Guan D, Wang Y (2013) Electrodeposition of Ag nanoparticles onto bamboo-type TiO<sub>2</sub> nanotube arrays to improve their lithium-ion intercalation performance. *Ionics* 19:879–885. doi:10.1007/s11581-012-0814-9
- Guan D, Li J, Gao X, Yuan C (2014a) Controllable synthesis of MoO<sub>3</sub>-deposited TiO<sub>2</sub> nanotubes with enhanced lithium-ion intercalation performance. *J Power Sources* 246:305–312. doi:10.1016/j.jpowsour.2013.07.096
- Guan D, Li J, Gao X, Yuan C (2014b) Effects of amorphous and crystalline MoO<sub>3</sub> coatings on the Li-ion insertion behavior of a TiO<sub>2</sub> nanotube anode for lithium ion batteries. *RSC Adv* 4:4055–4062. doi:10.1039/C3RA44849E
- Guo W, Xue X, Wang S, Lin C, Wang ZL (2012) An integrated power pack of dye-sensitized solar cell and Li battery based on double-sided TiO<sub>2</sub> nanotube arrays. *Nano Lett* 12:2520–2523. doi:10.1021/nl3007159
- <http://www.nature.com/srep/2013/130618/srep02007/abs/srep02007.html#supplementary-information>
- Kim HS, Kang SH, Chung YH, Sung Y-E (2010) Conformal Sn Coated TiO<sub>2</sub> nanotube arrays and its electrochemical performance for high rate lithium-ion batteries. *Electrochim Solid State Lett* 13:A15–A18. doi:10.1149/1.3264612
- Kyeremateng NA (2014) Self-organised TiO<sub>2</sub> nanotubes for 2D or 3D Li-ion microbatteries. *ChemElectroChem* 1:1442–1466. doi:10.1002/celec.201402109
- Kyeremateng NA, Lebouin C, Knauth P, Djenizian T (2013a) The electrochemical behaviour of TiO<sub>2</sub> nanotubes with Co<sub>3</sub>O<sub>4</sub> or NiO submicron particles: composite anode materials for Li-ion micro batteries. *Electrochim Acta* 88:814–820. doi:10.1016/j.electacta.2012.09.120
- Kyeremateng NA, Vacandio F, Sougrati MT, Martinez H, Jumas JC, Knauth P, Djenizian T (2013b) Effect of Sn-doping on the electrochemical behaviour of TiO<sub>2</sub> nanotubes as potential negative electrode materials for 3D Li-ion micro batteries. *J Power Sources* 224:269–277. doi:10.1016/j.jpowsour.2012.09.104
- Li W, Cheng F, Tao Z, Chen J (2006) Vapor-transportation preparation and reversible lithium intercalation/deintercalation of  $\alpha$ -MoO<sub>3</sub> microrods. *J Phys Chem B* 110:119–124. doi:10.1021/jp0553784
- Liu D et al (2008) TiO<sub>2</sub> nanotube arrays annealed in N<sub>2</sub> for efficient lithium-ion intercalation. *J Phys Chem C* 112:11175–11180. doi:10.1021/jp801300j
- Liu D et al (2009) TiO<sub>2</sub> nanotube arrays annealed in CO exhibiting high performance for lithium ion intercalation. *Electrochim Acta* 54:6816–6820. doi:10.1016/j.electacta.2009.06.090
- Liu S et al (2012) Nanosheet-constructed porous TiO<sub>2</sub>-B for advanced lithium ion batteries. *Adv Mater* 24:3201–3204. doi:10.1002/adma.201201036
- Matiko JW, Grabham NJ, Beeby SP, Tudor MJ (2014) Review of the application of energy harvesting in buildings. *Meas Sci Technol* 25:012002
- Meng X, Yao J, Liu F, He H, Zhou M, Xiao P, Zhang Y (2013) Preparation of SnO<sub>2</sub>@C-doping TiO<sub>2</sub> nanotube arrays and its electrochemical and photoelectrochemical properties. *J Alloys Compd* 552:392–397. doi:10.1016/j.jallcom.2012.10.177
- Moriguchi I, Hidaka R, Yamada H, Kudo T, Murakami H, Nakashima N (2006) A mesoporous nanocomposite of TiO<sub>2</sub> and carbon nanotubes as a high-rate Li-intercalation electrode material. *Adv Mater* 18:69–73. doi:10.1002/adma.200501366
- Patil A, Patil V, Wook Shin D, Choi J-W, Paik D-S, Yoon S-J (2008) Issue and challenges facing rechargeable thin film lithium batteries. *Mater Res Bull* 43:1913–1942. doi:10.1016/j.materresbull.2007.08.031
- Pikul JH, Gang Zhang H, Cho J, Braun PV, King WP (2013) High-power lithium ion microbatteries from interdigitated three-dimensional bicontinuous nanoporous electrodes. *Nat Commun* 4:1732. doi:10.1038/ncomms2747
- Qiu Y, Yan K, Yang S, Jin L, Deng H, Li W (2010) Synthesis of size-tunable anatase TiO<sub>2</sub> nanospindles and their assembly into anatase@titanium oxynitride/titanium nitride-graphene nanocomposites for rechargeable lithium ion batteries with high cycling performance. *ACS Nano* 4:6515–6526. doi:10.1021/nl101603g
- Reddy MV, Subba Rao GV, Chowdari BVR (2013) Metal oxides and oxysalts as anode materials for Li ion batteries. *Chem Rev* 113:5364–5457. doi:10.1021/cr3001884
- Ren Y, Liu Z, Pourpoint F, Armstrong AR, Grey CP, Bruce PG (2012) Nanoparticulate TiO<sub>2</sub>(B): an anode for lithium-ion batteries. *Angew Chem Int Ed* 51:2164–2167. doi:10.1002/anie.201108300
- Ryu W-H, Nam D-H, Ko Y-S, Kim R-H, Kwon H-S (2012) Electrochemical performance of a smooth and highly ordered TiO<sub>2</sub> nanotube electrode for Li-ion batteries. *Electrochim Acta* 61:19–24. doi:10.1016/j.electacta.2011.11.042
- Wang J, Zhou Y, Hu Y, O'Hayre R, Shao Z (2011) Facile synthesis of nanocrystalline TiO<sub>2</sub> mesoporous microspheres for lithium-ion batteries. *J Phys Chem C* 115:2529–2536. doi:10.1021/jp1087509
- Wang X, Xiang Q, Liu B, Wang L, Luo T, Chen D, Shen G (2013) TiO<sub>2</sub> modified FeS nanostructures with enhanced electrochemical performance for lithium-ion batteries. *Sci Rep*. doi:10.1038/srep02007
- Wu J, Hong H (2014) Investigation of metal oxide/carbon nanotubes as anode material for high capacity lithium-ion cells. *Meeting Abstracts MA2014-02:370*
- Wu HB, Chen JS, Hng HH, Wen Lou X (2012a) Nanostructured metal oxide-based materials as advanced anodes for lithium-ion batteries. *Nanoscale* 4:2526–2542. doi:10.1039/C2NR11966H
- Wu QL, Li J, Deshpande RD, Subramanian N, Rankin SE, Yang F, Cheng Y-T (2012b) Aligned TiO<sub>2</sub> nanotube arrays as durable lithium-ion battery negative electrodes. *J Phys Chem C* 116:18669–18677. doi:10.1021/jp3072266
- Xiong P, Liu B, Teran V, Zhao Y, Peng L, Wang X, Yu G (2014) Chemically integrated two-dimensional hybrid zinc

- manganate/graphene nanosheets with enhanced lithium storage capability. *ACS Nano* 8:8610–8616. doi:[10.1021/nm5041203](https://doi.org/10.1021/nm5041203)
- Xue L, Wei Z, Li R, Liu J, Huang T, Yu A (2011) Design and synthesis of Cu<sub>6</sub>Sn<sub>5</sub>-coated TiO<sub>2</sub> nanotube arrays as anode material for lithium ion batteries. *J Mater Chem* 21:3216–3220. doi:[10.1039/C0JM03819A](https://doi.org/10.1039/C0JM03819A)
- Yang M, Yang G, Spiecker E, Lee K, Schmuki P (2013) Ordered “superlattice” TiO<sub>2</sub>/Nb<sub>2</sub>O<sub>5</sub> nanotube arrays with improved ion insertion stability. *Chem Commun* 49:460–462. doi:[10.1039/C2CC37226F](https://doi.org/10.1039/C2CC37226F)
- Yu L, Wang Z, Zhang L, Wu HB, Lou XW (2013) TiO<sub>2</sub> nanotube arrays grafted with Fe<sub>2</sub>O<sub>3</sub> hollow nanorods as integrated electrodes for lithium-ion batteries. *J Mater Chem A* 1:122–127. doi:[10.1039/C2TA00223J](https://doi.org/10.1039/C2TA00223J)
- Yu X, Wang L, Liu J, Sun X (2014) Porous MoO<sub>3</sub> film as a high-performance anode material for lithium-ion batteries. *ChemElectroChem* 1:1476–1479. doi:[10.1002/celec.201402145](https://doi.org/10.1002/celec.201402145)
- Zhang Y, Yang Y, Xiao P, Zhang X, Lu L, Li L (2009) Preparation of Ni nanoparticle–TiO<sub>2</sub> nanotube composite by pulse electrodeposition. *Mater Lett* 63:2429–2431. doi:[10.1016/j.matlet.2009.08.019](https://doi.org/10.1016/j.matlet.2009.08.019)
- Zhao G, Zhang N, Sun K (2013) Electrochemical preparation of porous MoO<sub>3</sub> film with a high rate performance as anode for lithium ion batteries. *J Phys Chem A* 1:221–224. doi:[10.1039/C2TA00361A](https://doi.org/10.1039/C2TA00361A)
- Zhu Q, Hu H, Li G, Zhu C, Yu Y (2015) TiO<sub>2</sub> nanotube arrays grafted with MnO<sub>2</sub> nanosheets as high-performance anode for lithium ion battery. *Electrochim Acta* 156:252–260. doi:[10.1016/j.electacta.2015.01.023](https://doi.org/10.1016/j.electacta.2015.01.023)